Chemical Engineering Journal 313 (2017) 1468–1476

Contents lists available at ScienceDirect

Chemical Engineering Journal

journal homepage: www.elsevier.com/locate/cej

Microreactor with silver-loaded metal-organic framework films for gas-phase reactions

Rocío L. Papurello [a], José L. Fernández [b], Eduardo E. Miró [a], Juan M. Zamaro [a,*]

[a] Instituto de Investigaciones en Catálisis y Petroquímica, INCAPE (FIQ, UNL, CONICET), Santiago del Estero 2829, 3000 Santa Fe, Argentina
[b] Programa de Electroquímica Aplicada e Ingeniería Electroquímica, PRELINE (FIQ, UNL), Santiago del Estero 2829, 3000 Santa Fe, Argentina

HIGHLIGHTS

- Microreactors based on metal-organic framework films for gas-phase reactions.
- In-situ growth of homogeneous and stable ZIF-8 films on copper microchannels.
- ZIF-8 films activated with highly dispersed silver species.
- Microreactors with high activity and stability in the CO oxidation reaction.

GRAPHICAL ABSTRACT

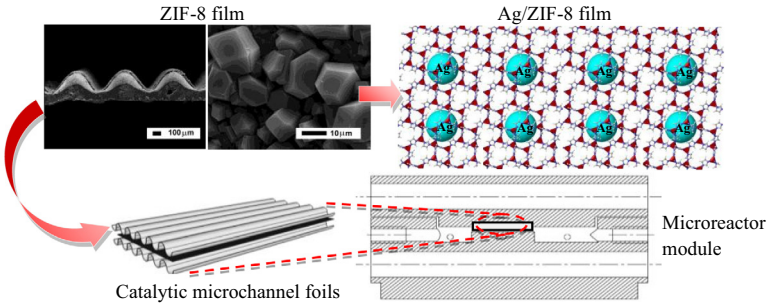

ARTICLE INFO

Article history:
Received 2 August 2016
Received in revised form 18 October 2016
Accepted 6 November 2016
Available online 8 November 2016

Keywords:
Micro-structured reactor
Ag/ZIF-8 film
In-situ growth
Catalytic coating
CO oxidation

ABSTRACT

Microreactors of copper foils with microchannels having zeolitic imidazolate framework-8 (ZIF-8) films were developed. The films were obtained by direct solvothermal synthesis on the microchannels; they presented micrometric thicknesses and homogeneity, and were activated with highly dispersed silver species. The MOF-based microreactors showed high activity and stability in the carbon monoxide oxidation, which is a benchmark for exothermic gas-phase reactions. The results could bring new perspectives in the development of microreactors for heterogeneous catalytic gas-phase reactions based on other MOF films as supports of active phases.

1. Introduction

Microreactors are structured catalytic systems with channels smaller than 500 μm that have an advantageous performance compared to other conventional catalytic configurations such as pellets or powders due to the higher mass and heat rates they can achieve [1]. Additionally, due to their high surface/volume ratio, short residence times are generated which increase selectivity and efficiency in many catalytic processes. As a result of these properties, microreactors can facilitate the control of highly endo or exothermic gas-phase reactions, which are difficult to be carried out in traditional reactors [2]. This type of devices enable featured performances in several catalytic processes, i.e. water gas shift reaction, alcohol steam reforming, selective methanation of carbon monoxide or preferential oxidation of CO [3]. Even though silicon and stainless steel are the materials most widely reported as substrates in the literature [4,5], the use of substrates with higher thermal conductivity and thermal diffusivity is an attractive alternative because they can improve the heat management towards or from the catalytic film [6]. For example, this has led to the development of microreactors based on substrates of aluminum or copper

* Corresponding author.
E-mail address: zamaro@fiq.unl.edu.ar (J.M. Zamaro).

http://dx.doi.org/10.1016/j.cej.2016.11.046
1385-8947/

alloys [7–9,12]. However, the deposition of adherent and homogeneous catalytic films on the surface of micro-channels is challenging, particularly on metallic substrates with low surface roughness. In order to address this issue, consistent alternatives have been proposed to carry out in situ growth of porous coatings with high specific surface area followed by the dispersion of the active species therein. Thus, zeolite film-based microreactors have been developed which have been highly effective in several catalytic reactions [10–13]. The above discussion explains our interest in developing new porous film-based microreactors, as one of the tools that could improve such technologies, for example in terms of dispersion and stabilization of active species. In recent years, continuous research in new porous materials has led to the development of Metal-Organic Frameworks (MOFs), which are crystalline solids consisting of inorganic clusters linked by organic ligands in three-dimensional arrangements. They have a unique chemical versatility, high internal porosity and properties different from those of traditional porous materials such as zeolites, porous silicas, or activated carbon [14]. A MOF's family with potential applications in solid-gas heterogeneous catalysis is that of zeolitic imidazolate frameworks (ZIFs) since they present high specific surface as well as good thermal and chemical stability [15,16]. ZIF-8 is an archetypical material of this kind, in which Zn^{2+} atoms are linked to nitrogens of imidazolate anions at connection angles close to 145° in tetrahedral coordination, forming a three-dimensional porous network with a zeolitic topology (SOD type) [17]. Supported ZIF-8 films have been studied mainly for adsorption and gas separation applications [18], whereas their use in heterogeneous catalysis remains as a largely unexplored area. Recently, a composite membrane microreactor made of ZIF-8/NaA films on multi-channel stainless steel plates has been applied in the continuous flow Knoevenagel condensation of benzaldehyde and ethyl cyanoacetate [19]. In other configurations, Fe_3O_4@ZIF-8 core-shell microspheres have been used in a capillary microreactor showing good catalytic activity for the same reaction [20]. Pd/ZSM-5@ZIF-8 core–shell structures have also been used for liquid phase hydrogenations of 1-hexene and cyclohexene [21]. To the best of our knowledge, no studies on microreactors based on metal-organic framework films for gas-phase heterogeneous catalytic reactions have been reported in the literature. However, there are a few reports of MOFs containing metal particles that were applied as catalysts for the CO oxidation reaction [22,23]. In the present work, we developed a microreactor based on films of the zeolitic imidazolate framework-8 (ZIF-8) on metallic microchannels as support for active species, which was applied in the CO oxidation reaction. The intention is to contribute to the development to film-based microreactors. The in-situ growth of MOF films, their functionalization with silver species and their catalytic assay in this model gas-phase reaction are also discussed.

2. Experimental

2.1. Microchannel conformation and synthesis of MOF films

Electrolytic copper foils (100 μm thickness) were cut in 2 × 2.5 cm pieces and then micro-folded employing a home-made device containing two rollers having micrometer sized teeth. In order to change the pressure on the foils and optimize the folding conditions, the space between these rollers was regulated. After that, the substrates were washed first with water and then with acetone in an ultrasonic bath after which the ZIF-8 growth was performed by direct solvothermal synthesis, using a protocol we have recently optimized to obtain films of this MOF on flat metallic substrates [24]. The reaction mixture consisted of $(NO_3)_2Zn{\cdot}6H_2O$ (Zn, Sigma Aldrich), sodium acetate (Ac, Cicarelli pro-analysis), 2-methylimidazole (Mim, Sigma Aldrich) and methanol (Cicarelli pro-analysis) in a molar ratio of Zn:Ac:Mim:methanol 1:2:2:2000. The reactants were stirred for 30 min and then placed in a Teflon vessel together with the microchanneled substrate; the synthesis treatments were carried out at 120 °C between 1 and 24 h. Later, the substrates were removed, treated in an ultrasonic bath for 30 s to eliminate residues from the surface, and finally dried at 70 °C.

2.2. Sample characterization

The formation of microchannels was examined by optic microscopy (OM) with a Leica S8 APO stereomicroscope with a Leica LC3 digital camera. Representative cross-section micrographs of the substrates were obtained and measurements were made to determine the fundamental dimensions of the microchannels. The microstructure of the MOF films was examined by scanning electron microscopy (SEM) with a JEOL JSM-35C operated at 20 kV. The samples were glued to the sample holder with Ag painting and then coated with a thin layer of sputtered Au in order to improve the images. For the elemental mapping of the microreactor surfaces a FEG-SEM FEI NanoNova 230 was employed, operated at an acceleration voltage of 20 kV. Diffuse reflectance infrared spectroscopy (DRIFT) was performed with a Shimadzu Prestige 8101 M (40 scans, resolution 2 cm^{-1}) in order to analyze vibrational modes of the films. The crystalline structure of the growths was analyzed trough X-ray diffraction (XRD) with a Shimadzu XD-D1 instrument (CuKα radiation, λ = 1.5418 Å, 2 °C min^{-1}, 30 mV, 40 mA, 2θ = 5° to 50°). Calculations of Crystallographic Preferred Orientation (CPO) were made by means of the formula: $CPO\frac{x}{y} = \frac{(If^x - If^y) - (Ip^x - Ip^y)}{(If^x - If^y)}$ where I is the integrated intensity, f denotes the signal in the film, p denotes the signal in the powder, x and y denotes the considered planes [25]. The substrate surface was examined by atomic force microscopy (AFM) with an Agilent 5400 (Keysight Technologies) with a standard cantilever in intermittent contact-mode obtaining topography and phase images. The surface composition of films was examined by X-ray photoelectron spectroscopy (XPS) with a Multitechnique Specs module. The binding energies (BE) of Ag3d, Cu2p, Zn2p, C1s, N1s and O1s core-levels were analyzed. The kinetic energy (KE) in the CuLMM, AgMNN and ZnLMM regions transitions was also analyzed. The spectra were obtained with a pass energy of 30 eV with a Mg anode operated at 200 W. The foils were supported on the sample holder, subjected to vacuum dehydration at 150 °C for 15 min and finally evacuated under vacuum, prior to the readings. The peak of C1s at 284.8 eV was taken as internal reference. Data processing was performed using the Casa XPS software.

2.3. Activation and evaluation of MOF films in a microreactor

Silver was introduced in the films by quasi-incipient wetness impregnation through the dripping of exact amounts of silver nitrate ethanolic solutions of known concentrations (0.01 0.02 0.03 M), adding dropwise onto the film an exact volume of these solutions to obtain the required mass of Ag. Subsequently, films were exposed under UV radiation (TUV 15 W T8, Philips, 254.3 nm, 2.3 W m^{-2}, 30 min). Catalysts with different silver contents were thus obtained. Then, Ag/ZIF-8 supported films were stacked inside a microreactor module placing a flat plate (stainless steel) between two catalytic foils as shown in the scheme of the microreactor assembly in Fig. 1. The module counts with heating cartridges and a PID temperature controller, and reactant gases were dosed by mass flow controllers (Brooks Instruments 4800 series). The CO conversions were determined with an on-line Shimadzu GC-2014 chromatograph equipped with a TCD detector

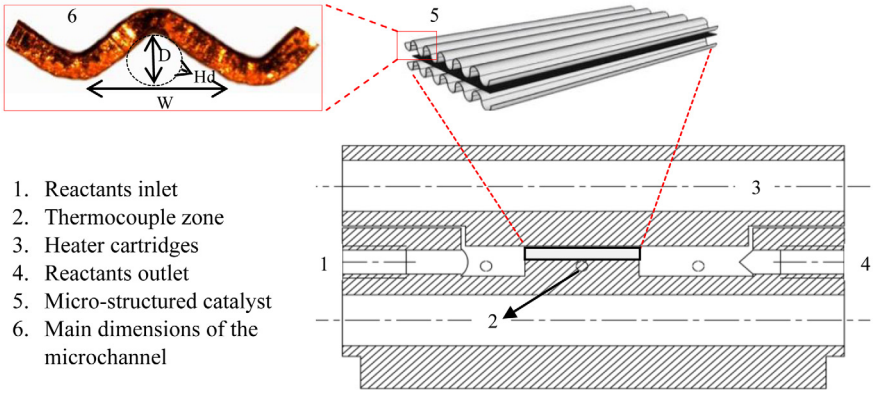

Fig. 1. Scheme of axial cross-section of the microreactor module, showing the housing section in which the catalytic microchannel foils are stacked. The micrograph inset shows the main dimensions of the microchannels.

and a 5A molecular sieve column. The composition of the reaction mixture was 1% CO, 2% O_2 in He balance with a total flow of 30 $cm^3\ min^{-1}$. Prior to the catalytic tests, the microreactors were treated in He (30 mL min^{-1}) between room temperature and 200 °C (5 °C min^{-1}) and maintained at that temperature for 60 min. CO conversions (X_{CO}) were calculated as: $X_{CO} = \frac{(CO^0 - CO)}{CO^0}$; where $[CO]^0$ and [CO] are inlet and outlet gas concentrations (mol cm^{-3}), respectively. The reaction rate was estimated taking into account conversion levels <15% through $r = \frac{C^0_{CO} \cdot X_{CO}}{W_{Ag}/F}$, where W_{Ag} is the amount of silver loaded in the microreactor (mg) and F is the gas flow ($cm^3\ s^{-1}$). In addition, pseudo-first order kinetic constants (k) were calculated at different temperatures as: $k = \frac{-l\ n\ (1-X_{CO})}{W_{Ag}/F}$.

3. Results and discussion

3.1. Conformation of microchannels

The microfolding of the substrates was adjusted by analyzing micrographs of cross sections of the samples. From these micrographs, the main dimensions of the microchannels were obtained, such as the width between the crests (W), depth (D), aspect ratio (A = W/D) and hydraulic diameter (Hd). As shown in Fig. 2, a good uniformity in the dimensions of the microchannels was achieved, since both W and D presented a normal-type distribution profile, with a low standard deviation. The average value of D was 218 ± 20 μm (Fig. 2a) and a slight right asymmetry in the histogram was noticed, while W was 717 ± 20 μm with a slight deviation of the distribution to the left (Fig. 2b). These dimensions provided an A value of about 3. This good conformation of the 54 microchannels per substrate obtained by this method was probably promoted by the high malleability of the copper foils. The hydraulic diameter (Hd) is a characteristic parameter which represents more realistically the flow behavior of reagents through the channels. By approximating the cross section of the microchannels to a triangular shape, an Hd was estimated through the relationship Hd = 4S/P [26], wherein S and P represent the area of the channel section and its perimeter, respectively. In this way, microchannels with Hd around 201 ± 16 μm were obtained with a slight positive bias of the distribution curve (Fig. 2c). Considering the flow conditions of the gases in the catalytic test, this will provide the development of a laminar flow (Re = 925) where the Reynolds number was calculated as $Re = \frac{\rho v_s Hd}{\mu}$ ρ being the density of fluid, μ the dynamic viscosity, v_s the fluid velocity and Hd the hydraulic diameter.

3.2. In-situ growth of MOF films on the microchannels

Recently, we needed to apply the secondary synthesis (SS) approach to obtain a selective growth of uniform ZIF-8 films on flat copper substrates [24] since by direct synthesis (DS) continuous films were not developed. In contrast, in the present case, after subjecting the copper substrates with microchannels to a direct synthesis for 10 h, the development of a pure ZIF-8 phase on its surface was obtained. This was verified by the presence of all XRD indexed signals for this MOF, in addition to the intense signal of the substrate (Fig. 3). Moreover, such MOF signals matched the diffraction pattern of the crystals recovered from the synthesis solution. By reducing the treatment time to 6 h, all the ZIF-8 diffraction peaks can still be detected with appreciable intensity and are even clearly defined in the sample treated for 2 h. It can be seen that the intensity of the XRD peaks evolves with increasing time. However, in the sample obtained at 20 h no noticeable changes can be observed in the diffractogram compared with the sample at 10 h, suggesting that modifications no longer occur in the growth of the MOF film (Fig. 3). Moreover, the relative intensities of the main XRD signals of the films are similar to those of the recovered powder. By comparing the relationship between the integrated intensities of the ⟨1 1 0⟩, ⟨2 0 0⟩ and ⟨2 1 1⟩ planes from the growths and those from the powder, the crystallographic preferential orientation indexes (CPO) (110/200) and (211/200) take values near zero. This indicates a random distribution of the MOF crystals on the substrate surface, which is a typical behavior of crystalline growths obtained by DS. Such feature contrasts with that obtained in ZIF-8 films developed by SS on this type of substrate, which have a strong preferential crystallographic orientation.

Fig. 4 shows a SEM image of the sample obtained at 10 h exhibiting a uniform growth of crystals that completely covers the microchannels, with mean crystal size of about 12 μm and a film thickness of similar dimensions. The thickness was similar throughout the entire substrate surface, both at the bottom and at the top of each microchannel (inset Fig. 4). Moreover, no differences in either crystal size or film thickness were observed for the sample synthesized at 20 h, in agreement with the XRD results. Comparing these growths with those obtained by SS under similar synthesis conditions (time and temperature), no significant differences were noticed in terms of crystal size and thickness of the film, although the extension of the intergrowth clearly changed. These films showed a somewhat lower intergrowth producing more defined individual crystals, as shown in Fig. 4. In the sample obtained after 6 h treatment, a uniform and continuous film was also observed, although the crystal size and film thickness were

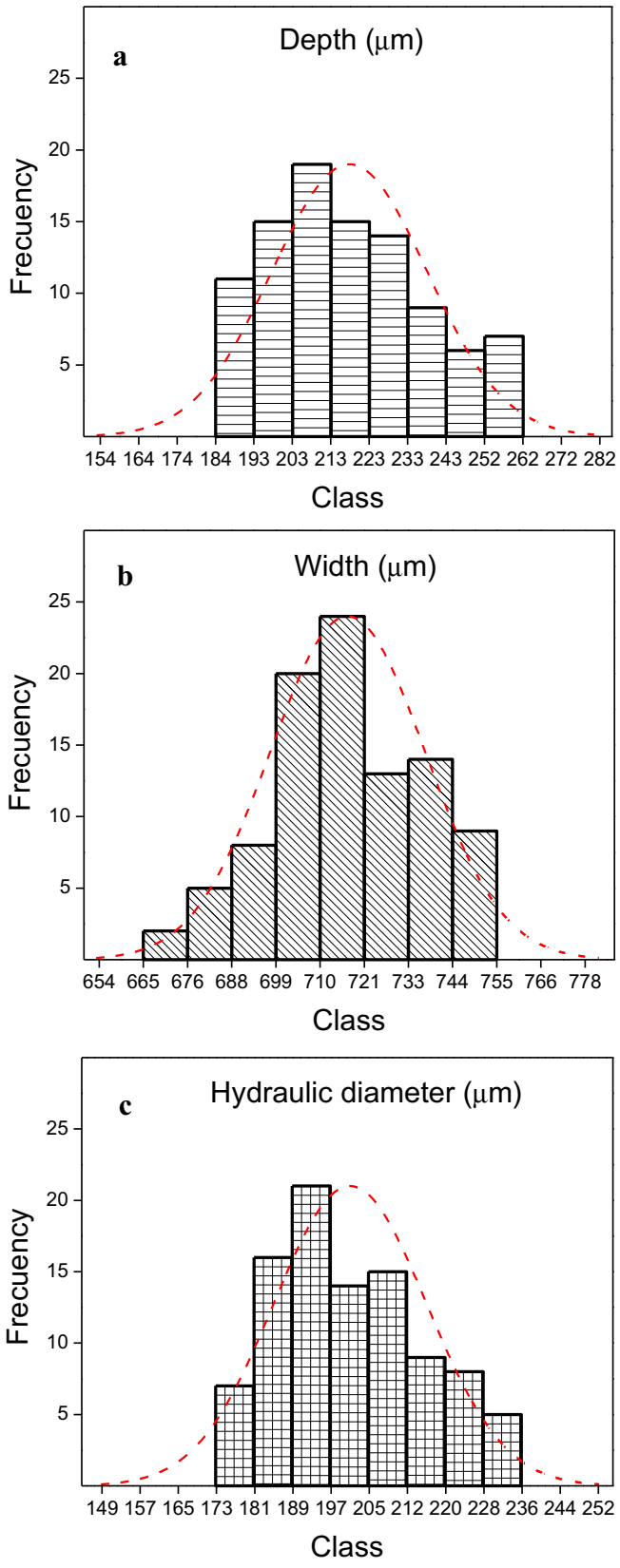

Fig. 2. Distribution histograms of the characteristic dimensions of the microchannels obtained by microfolding: a) Depth, b) Whidt, c) Hydraulic diameter in microns.

reduced to about 8 μm. Moreover, for a treatment time of 2 h, small crystals of about 5 μm grew homogeneously dispersed in the microchannels but without forming a continuous film

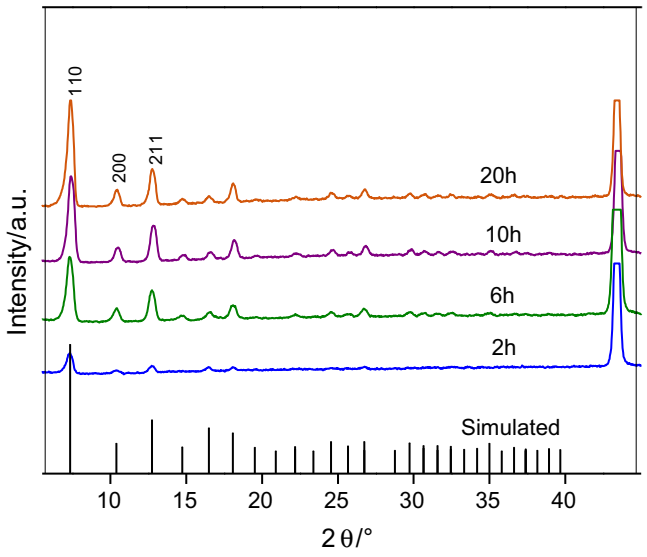

Fig. 3. XRD patterns of the growths obtained by direct synthesis at different treatment times. A theoretical ZIF-8 pattern simulated from CCDC archive (602538) is also displayed.

(Fig. 4). In correlation with XRD results, the SEM images of this sample show that an incipient crystal growth was produced with some cube-shaped crystals, which began to adopt the typical dodecahedral shape of ZIF-8 crystals in line with the morphology of this MOF at the early stages of growth [27]. The direct syntheses on copper microchannels in open configuration, fully exposed to the synthesis medium, allowed obtaining uniform MOF films without inhomogeneous deposits which are optimal to be used in a microreactor. The 10-h sample showed an optimal quality with a coverage of about 0.4 mg cm^{-2} of substrate surface area. Moreover, the high porosity of this film was confirmed which showed a specific surface area (BET) of about 1417 $m^2 g^{-1}$ that was almost identical to that of the ZIF-8 powder (1432 $m^2 g^{-1}$). The mechanical stability is another important quality these films must meet in view of their application in a gas stream. In this regard, a high adhesion was noticed since no detachment occurred with the ultrasound treatment performed during the cleaning after the film synthesis and a strong anchorage to the substrate was also observed after the cuts made for SEM observations. Previously, exhaustive adherence studies of the ZIF-8 films were carried out, which showed a high adhesion after being subjected to long ultrasound treatments and thermo-mechanical cycles in muffle followed by the ultrasound test [24].

The dense crystal growth obtained at short synthesis times suggests a promotion of the MOF nucleation on the substrate surface. The 3D topographic profile of the microchannel surface shows a fine grain nanostructure (Fig. 5a-i) which is typical of copper electrodeposits, in agreement with the origin of this commercial substrate obtained by lamination of electrolytic copper deposits. However, the size of these grains is much smaller and they are in a higher proportion in the substrate with microchannels compared to the original flat foil (not shown), which most likely originates from the high compression suffered by the substrate during the folding process. The creation of this nanoroughness on the microchannels surface fosters the development of the film by providing a high density of nucleation sites for the MOF. Meanwhile, the 3D surface profile of the microchannel which was solvothermically treated for 1 h, shows a modification of the surface structure (Fig. 5a-ii) having nanometric formations most probably nuclei of the MOF in early stages which are deposited on a somewhat

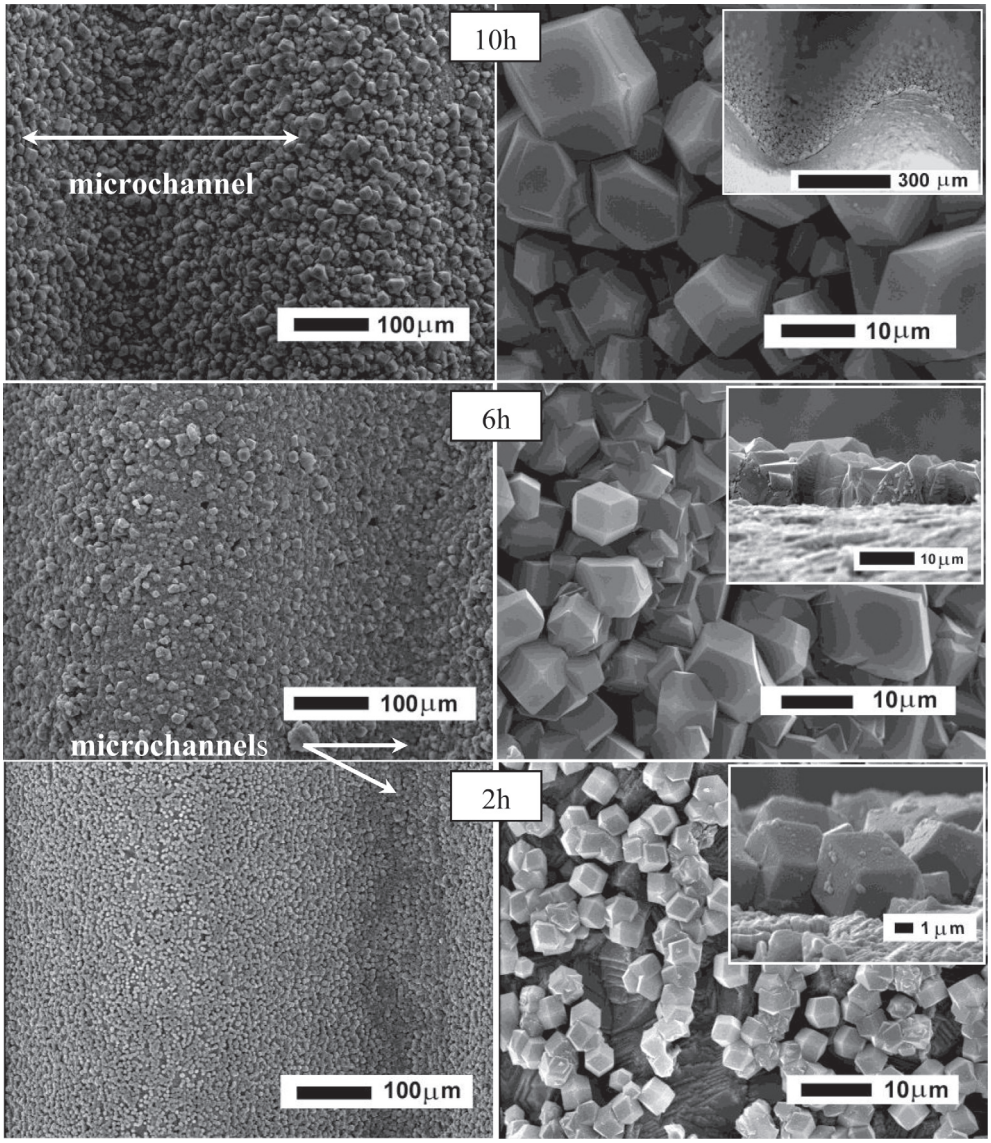

Fig. 4. SEM micrographs of the microchannels with ZIF-8 films synthesized at different times.

smoother surface. The latter is associated with a partial dissolution of the substrate that occurs during the solvothermal treatment under the present conditions. The SEM images of this sample also confirm the presence of small particles scattered on the substrate surface (Fig. S1). The height profiles plotted on AFM topographical images (Fig. 5b-i) indicate that these formations have heights between 5 and 20 nm and basal diameters between 10 and 50 nm. Moreover, the phase images (Fig. 5b-ii) confirm that such deposits are of a chemical nature different from that of the substrate, proving the hypothesis that these formations correspond to the MOF at the early stages of growth. These findings are in agreement with studies of ZIF-8 crystal growth in methanol, which indicated a rapid evolution of the MOF formation with a high crystallinity at short synthesis times (30–40 min), where the first crystals can be observed [28].

3.3. Film activation and evaluation in a microreactor

In recent years it has been well-established, on the one hand, that Ag nanosized catalysts display good low-temperature CO oxidation and reaction stabilities [29] and, on the other hand, that several types of MOFs can support silver species forming molecular-scale clusters distributed uniformly throughout the MOF crystals [30]. Based on the above, we incorporated silver as active center in the ZIF-8-based microreactors, denoted as Ag (x)/ZIF-8/MR, where (x) indicates the silver loading (mg) and MR means microreactor.

The XRD patterns of the fresh silver loaded microreactors show that during the impregnation process the structure of the MOF films was unchanged and no extra signals appeared (Fig. 6) indicating that silver species were highly dispersed in the films. DRIFT spectra of these same films also show that the bond structure of the MOF remains intact (Fig. S2), confirming its structural integrity after the silver impregnation. The microreactors were evaluated in the CO oxidation from room temperature up to 300 °C, as these films proved to be structurally stable under inert atmosphere up to about 350 °C [24]. The obtained CO conversions are shown in Fig. 7, where results found with the bare ZIF-8/MR microreactor are also included for comparison. During the growth of ZIF-8 over the copper foil, some amount of Cu is leached from the substrate and part of it remains into the film structure [24]. In addition, we performed EDS analyses and elemental line scan on transversal cuts of this sample, which confirmed the presence of copper in the MOF film (Fig. S3).

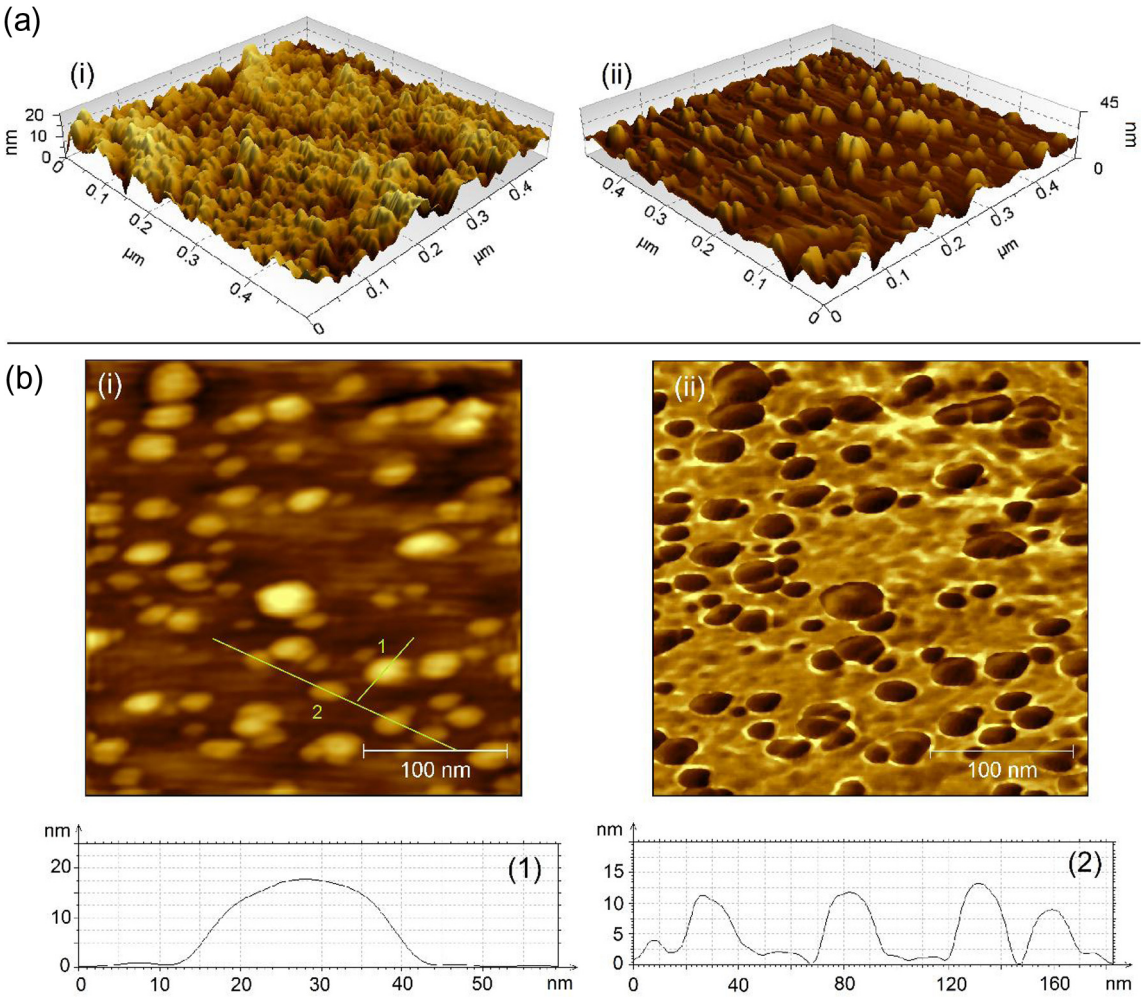

Fig. 5. (a) 3D representation of the topographic AFM images: (i) microfolded copper foil; (ii) microfolded copper foil subjected to a solvothermal treatment for 1 h. (b) AFM topographic (i) and phase (ii) images of the copper foil treated at 1 h. The height profiles (1) and (2) were taken on image b-(i).

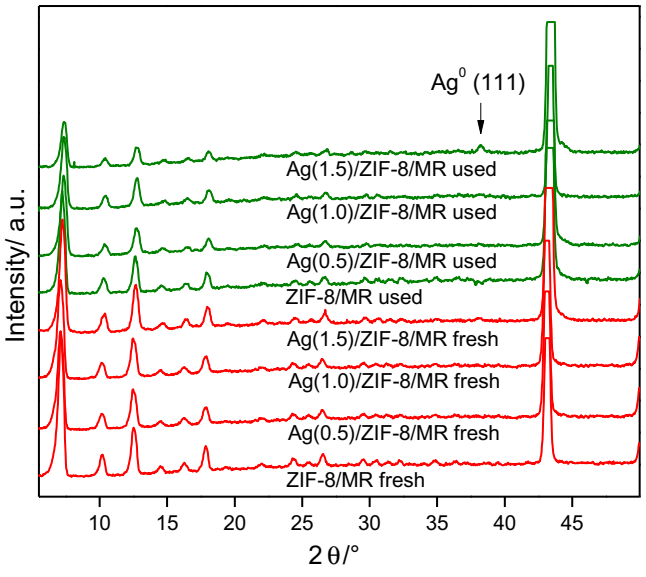

Fig. 6. XRD patterns of the microreactors after and before the catalytic assays.

Thus, the bare ZIF-8/MR itself develops CO oxidation activity reaching the temperature for 50% of CO conversion (T^{50}) at 280 °C. This activity is associated with dispersed copper species in the MOF film, since it has been demonstrated that ZIF-8 crystals are inactive for this reaction [22]. Moreover, we show that after the impregnation of a small amount of silver, the CO conversion increased (Fig. 7) for Ag(0.5)/ZIF-8/MR, reaching T^{50} at 250 °C as a consequence of the activities of both copper and silver species. In order to investigate the activity of these microreactors, two other catalysts with higher silver loadings were tested; they were denoted Ag(1.0)/ZIF-8/MR and Ag(1.5)/ZIF-8/MR. As shown in Fig. 7, the T^{50} was 210 °C and 225 °C, respectively. Interestingly, the CO oxidation activity increased when the silver loading increased from 0.5 mg to 1.0 mg, but the same effect was not observed for the microreactor loaded with 1.5 mg. Reaction rates calculated at 200 °C take similar values when comparing Ag(0.5)/ZIF-8/MR (6.10^{-5} mol.s^{-1}.g^{-1}) and Ag(1.0)/ZIF-8/MR (7.10^{-5} mol.s^{-1}.g^{-1}) but decrease for the Ag(1.5)/ZIF-8/MR sample (4.10^{-5} mol.s^{-1}.g^{-1}). These results indicate that for lower loadings, active silver species are readily accessible in the ZIF-8 porous films, but with higher silver amounts metal species probably either block the ZIF-8 pores or sinterize. The reaction rate value calculated for the best catalytic microreactor among those studied in this work (Ag(1.0)/ZIF-8/MR) is higher than that calculated from data

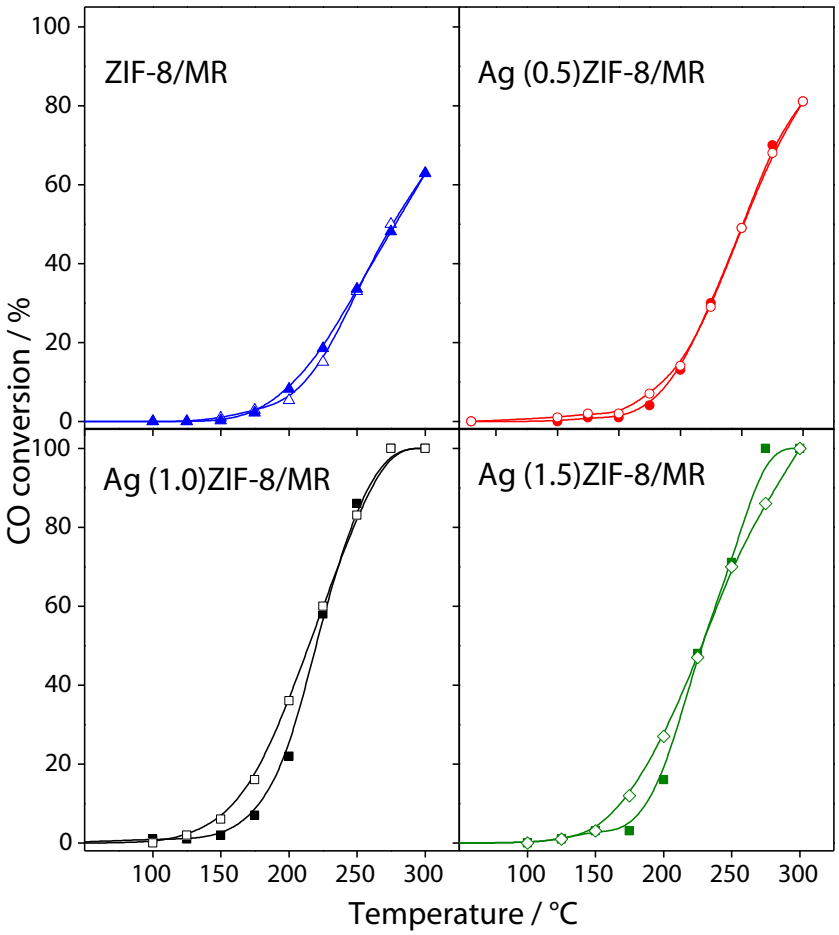

Fig. 7. Catalytic behavior of microreactors based on ZIF-8 films for the CO gas-phase oxidation. Plot of experiment at increasing temperatures (filled symbols) and of experiment at decreasing temperatures (open symbols).

extracted from the literature [23] for Ag-MOF (3.10^{-5} mol.s^{-1}.g^{-1}) and somewhat lower than that of the active gold supported in ZIF-8 (1.10^{-4} mol.s^{-1}.g^{-1}) [22]. For each evaluated microreactor, the catalytic experiments were performed by duplicate and the results were highly repetitive. As shown in Fig. 7, CO conversions were measured increasing the temperature up to 300 °C and then decreasing it in the opposite way; besides, a hysteresis loop was observed for Ag(1.0)/ZIF-8/MR and Ag(1.5)/ZIF-8/MR. This phenomenon has been frequently reported in the literature for CO oxidation on supported metallic catalysts and it can be ascribed to kinetic behaviors [31] or changes in the structure of the active sites [32]. In our case, given the reversibility observed of the hysteresis loop in consecutive evaluations, structural changes of the active phase are discarded. For the most active sample, Ag(1.0)/ZIF-8/MR, pseudo-first order kinetic constants (k) were calculated using CO conversions lower than 15% and the Arrhenius plot was built as shown in Fig. 8. By linearization, the activation energy (Ea) was obtained, which presented a value according to that reported in the literature for nano-silver catalysts (supported on SiO_2) in this reaction [33] and demonstrates the absence of diffusive constraints in the MOF film. The catalytic results show the effective implementation of the MOF-based microreactors for this highly exothermic reaction, having a high activity and stability in the reaction. MOF films allow the proper dispersion of silver species, acting as an effective support for stabilizing and preventing their agglomeration during the reaction. Following the catalytic tests, stability was evaluated by keeping the catalytic films under reaction atmosphere at high conversion levels for a period of 24 h. As shown for the most active microreactor (inset in Fig. 8), the conversion was maintained over time and even a slight increase was noticed, demonstrating a long-term stability behavior.

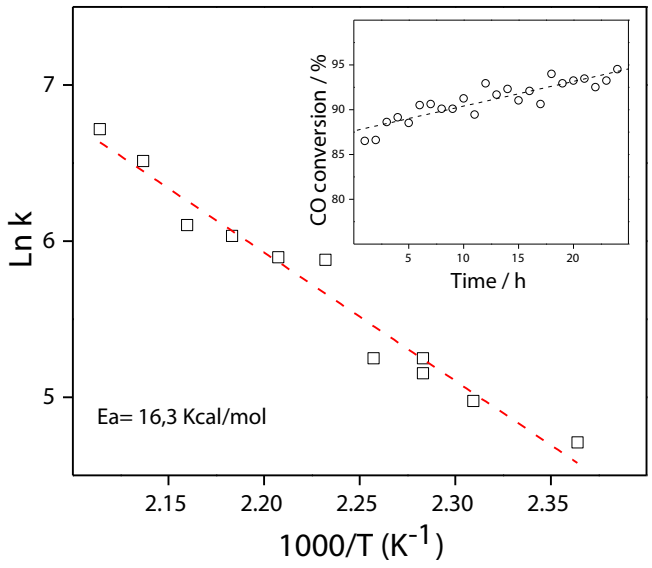

Fig. 8. Arrhenius plot for Ag(1.0)/ZIF-8/MR and estimation of the activation energy. Inset: time-on-stream stability experiment.

After the catalytic tests the units were disassembled and characterized by XRD (Fig. 6) and DRIFT. Fig. S2 shows the DRIFT spectrum of samples which were cycled in catalytic evaluation ramps. In agreement with the catalytic behavior, the spectrum reflects the physicochemical integrity of the film subjected to reaction since all characteristic vibrational modes of the ZIF-8 are observed, keeping the bond connectivity in the MOF intact. The imidazolate structure remained unchanged in view of the absence of the typical intense imidazole absorption band in the 2250–3300 cm^{-1} region and its associated signal at 1850 cm^{-1} [34]. Furthermore, the CH bending mode of the imidazolate was observed at 1147 cm^{-1} and also the rest of the MOF's bond structure remained unchanged, as the stretching mode of C=N at 1585 cm^{-1} and the bands in the 1350–1500 cm^{-1} region associated with the vibration of the ring [35]. The diffractograms of the evaluated microreactors (Fig. 6) confirmed that the structural integrity of the crystalline structure of the MOF remained unchanged with highly dispersed phases of silver in view that no signals of silver appeared in the Ag(0.5)/ZIF-8/MR and Ag(1.0)/ZIF-8/MR samples. However, in the Ag(1.5)/ZIF-8/MR sample a weak Ag^0 signal was observed at 38.1 ° (JCPDS 4-783) pointing to a certain agglomeration of silver particles in agreement with the reduction in the reaction rate observed for this sample.

The XPS analysis of both the microreactor without silver, ZIF-8/MR, and the more active Ag(1.0)/ZIF-8/MR, demonstrated the presence of copper on the MOF crystal surface, which was higher in the Ag(1.0)/ZIF-8/MR sample (Fig. S4). In this case, the Cu2p signals exhibit an acute shape with no satellites, which together with the Auger parameter (α) calculated from the spectrum in the CuLMM region, indicate the presence of Cu^{1+} in both the fresh and used samples (Table 1), which is due to a partial lixiviation of the substrate during synthesis. They are highly dispersed, as they were not detected by XRD. On the other hand, the small amount of surface copper in the ZIF-8/MR samples (about 0.01% Cu), makes it difficult to calculate α, although its presence explains the activity of this microreactor.

The Ag(1.0)/ZIF-8/MR sample shows electronic transitions of Ag3d (Fig. S4) with similar values of binding energies (BE) in the fresh and evaluated microreactor (Table 1). Since it is difficult to distinguish the oxidation state of silver species in this region, the Auger parameter was obtained from the AgMNN transitions which yielded a value of 726.2, thus confirming the presence of Ag^0 species both in the fresh and used samples [36]. Besides, the concentration of surface silver remained constant (about 0.02% Ag). This confirms the stability of those species, without surface segregation or change in their characteristics. The N/Zn ratio in all samples was

Table 1
XPS results of the ZIF-8-based microreactors.

	BE Cu $2p_{3/2}$ (FWHM)[a]	KE Cu LMM[b]	α'[c]	BE Ag $3d_{3/2}$ (FWHM)[a]	KE Ag MNN[b]	α'[d]	BE Zn $2p_{3/2}$ (FWHM)[a]	KE Zn LMM[b]	BE O 1s (FWHM)[a]	N/Zn
ZIF-8/MR fresh	932.9 (2.4)	*	*	–	–	–	1021.7 (2.5)	987.4	531.6 (2.8)	2.8
ZIF-8/MR used	932.8 (2.5)	*	*	–	–	–	1021.5 (2.5)	987.6	531.2 (3.0)	2.2
Ag(1.0)ZIF/MR fresh	932.7 (2.2)	915.9	1848.6	368.2 (1.4)	357.8	726.2	1021.9 (2.6)	988.6	531.3 (3.0) 530.4 (1.4)	1.8
Ag(1.0)ZIF/MR used	932.2 (2.4)	916.1	1848.4	367.9 (1.5)	358.3	726.2	1021.4 (2.5)	988.5	531.2 (2.7) 529.7 (2.3)	5.5

[a] Binding energy (BE) in eV.
[b] Kinetic energy (KE) in eV.
[c] Modified Auger parameter: α′ = KE (Cu LMM) − KE (Cu $2p_{3/2}$) + 1253.6 eV.
[d] Modified Auger parameter: α′ = KE (Ag MNN) − KE (Ag $3d_{3/2}$) + 1253.6 eV.
* Very small signals that do not allow the parameter calculation.

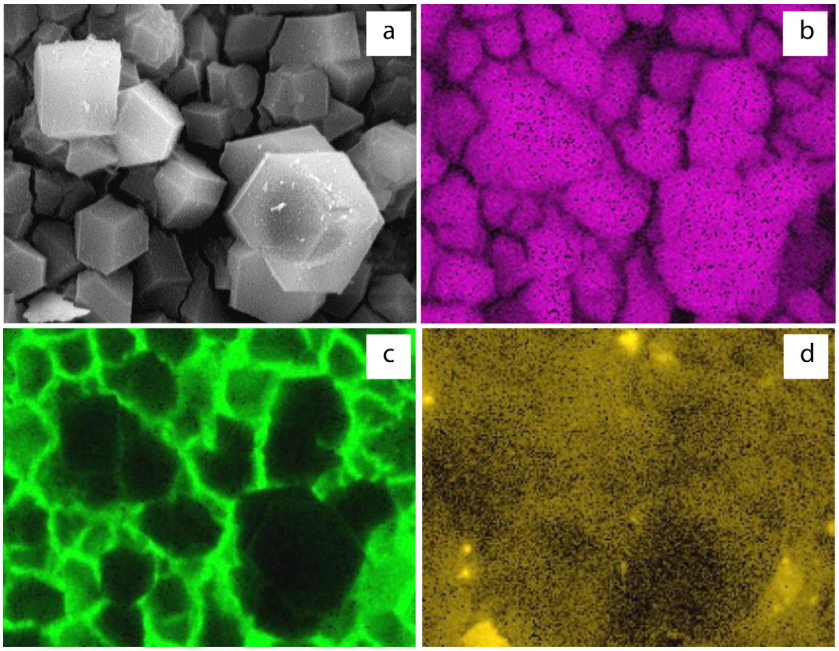

Fig. 9. X-ray mapping image of the Ag(1.0)/ZIF-8/MR sample before reaction: (a) SEM of the analyzed sector; (b) Cu mapping; (c) Zn mapping; (d) Ag mapping.

similar to that of the coatings obtained by SS [24] and somewhat smaller than the theoretical one, which suggests Zn enrichment. Nevertheless, in the evaluated silver-loaded sample that ratio increased twofold (Table 1). Moreover, the signals in the O1s region can be correctly adjusted with two components (Table 1), one around 530 eV in agreement with Cu and Zn oxides [37] and another around 531 eV which can be associated with surface hydroxides, without discarding the contribution of some oxygen of acetate species remaining from the synthesis. The presence of surface zinc oxide was confirmed for the fresh and used Ag(1.0)/ZIF-8/MR samples in view that the KE of the electronic transition in the ZnLMM Auger region was around 988.6 eV [37]. On the contrary, for the ZIF-8/MR samples, these signals were located at 987.6 eV, in agreement with zinc in the ZIF-8 structure [24].

The elemental X-ray mapping of the evaluated Ag(1.0)/ZIF-8/MR sample taken over a sector of the film as shown in Fig. 9a, indicates a uniform distribution of Zn as a consequence of the homogeneous coverage of the substrate with crystals of this MOF (Fig. 9b). The presence of a certain amount of Cu in the crystals was also observed (Fig. 9c) although its higher concentration was noticed at the slightly separated intercrystalline voids which were magnified during the long-lasting mapping acquisition. On the other hand, silver was distributed very evenly in the MOF films, although some deposits were observed in intercrystalline regions as a consequence of the impregnation process (Fig. 9d). Even though there are some reports that use TEM analyses for the study of metal particles in MOFs, it has been reported that TEM induces MOF degradation leading to the agglomeration of the initially formed particles, so it cannot provide true information about either the size or the location of the nanoparticles [38]. The silver distribution in our microreactors agrees well with the XRD, EDS mapping and XPS results and confirms the high dispersion of this active phase properly stabilized in the microporous structure of the MOF, even after being subjected to repeated catalytic tests, in correspondence with the high in-reaction activity and stability that this sample exhibited.

4. Conclusions

Uniform microchannels in copper foils were obtained employing a microfolding procedure, which showed uniformity in their characteristic dimensions with hydraulic diameters of about 200 μm. Subsequently, on these substrates it was possible to obtain homogeneous films, a few micron thick, of the Zeolitic Imidazolate Framework-8 (ZIF-8) through direct in-situ growth. The term "homogeneous" refers to the uniform growth of crystals that completely covers the microchannels, with a similar thickness along the substrate, which is an optimum condition for a catalytic application. The presence of a nanostructured surface in the substrate provided a high density of nucleation sites for the MOF, generating a uniform and well-anchored growth of crystals that completely covers the microchannels. Subsequently, such films were functionalized with silver species as active centers through the impregnation with silver solutions; then, they were successfully applied in a microreactor for CO oxidation. The microreactors showed a high activity and stability in this highly exothermic gas-phase reaction, as a consequence of the fact that the ZIF-8 films allow a high dispersion of the active phases avoiding their sintering and keeping unchanged the metal-organic framework structure during the reaction. MOFs have a high surface area, adjustable pore size and shape, and possibility of functionalization of their porous walls. Therefore, the results of this work can open new opportunities for the application of other MOF films as carriers of active species in catalytic heterogeneous gas-phase reactions using microreactors.

Acknowledgments

The authors thank the financial support received from CONICET, ANPCyT (PICT 1299) and Universidad Nacional del Litoral (CAI+D 486) for carrying out this study. Thanks are also given to Fabio Fontanarrosa for the SEM analyses.

Appendix A. Supplementary data

Supplementary data associated with this article can be found, in the online version, at http://dx.doi.org/10.1016/j.cej.2016.11.046.

References

[1] G. Kolb, V. Hessel, Chem. Eng. J. 98 (2004) 1–38.
[2] L. Kiwi-Minsker, A. Renken, Catal. Today 110 (2005) 2–14.
[3] G. Kolb, Chem. Eng. Process. 65 (2013) 1–44.
[4] P. Mills, D. Quiram, J. Ryley, Chem. Eng. Sci. 62 (2007) 6992–7010.
[5] Z. Boukha, J. Ayastuy, A. Iglesias-González, B. Pereda-Ayo, M. Gutiérrez-Ortiz, J. González-Velasco, Appl. Catal., B 160–161 (2014) 629–640.
[6] G. Groppi, G. Airoldi, C. Cristiani, E. Tronconi, Catal. Today 60 (2000) 57–62.
[7] I. Ismagilov, E. Michurin, O. Sukhova, L. Tsykoza, E. Matus, M. Kerzhentsev, Z. Ismagilov, A. Zagoruiko, E. Revrov, M. de Croon, J. Schouten, Chem. Eng. J. 135S (2008) S57–S65.
[8] P. Pfeifer, K. Schubert, M. Liauw, G. Emig, Appl. Catal., A 270 (2004) 165–175.
[9] C. Horny, L. Kiwi-Minsker, A. Renken, Chem. Eng. J. 101 (2004) 3–9.
[10] V. Sebastian, S. Irusta, R. Mallada, J. Santamaría, Catal. Today 147S (2009) S10–S16.
[11] Y. Wan, J. Chau, K. Yeung, A. Gavriilidis, J. Catal. 223 (2004) 241–249.
[12] N. Pérez, E. Miró, J. Zamaro, Appl. Catal., B 129 (2013) 416–425.
[13] L. Truter, V. Ordomsky, J. Schouten, T. Nijhuis, Appl. Catal., A 515 (2016) 72–82.
[14] G. Férey, Chem. Soc. Rev. 37 (1) (2008) 191–214.
[15] J. Rowsell, O. Yagui, Microporous Mesoporous Mater. 73 (1–2) (2004) 3–14.
[16] Y. Tian, S. Yao, D. Gu, K. Cui, D. Guo, G. Zhang, Z. Chen, D. Zhao, Chem. Eur. J. 16 (2010) 1137–1141.
[17] A. Phan, C. Doonan, F. Uribe-Romo, C. Knobler, M. O'Keeffe, O. Yaghi, Acc. Chem. Res. 43 (2010) 58–67.
[18] A. Bétard, R. Fischer, Chem. Rev. 112 (2012) 1055–1083.
[19] G. Zhang, T. Zhang, X. Zhang, K. Yeung, Catal. Commun. 68 (5) (2015) 93–96.
[20] T. Zhang, X. Zhang, X. Yan, L. Kong, G. Zhang, H. Liu, J. Qiu, K. Yeung, Chem. Eng. J. 228 (2013) 398–404.
[21] T. Zhang, X. Zhang, X. Yan, L. Lin, H. Liu, J. Qiu, K. Yeung, Catal. Today 236 (2014) 41–48.
[22] H. Jiang, B. Liu, T. Akita, M. Haruta, H. Sakurai, Q. Xu, J. Am. Chem. Soc. 131 (2009) 11302–11303.
[23] X. Qian, Z. Zhong, B. Yadian, J. Wub, K. Zhou, Int. J. Hydrogen Energy 39 (2014) 14496–14502.
[24] R. Papporello, E. Miró, J. Zamaro, Microporous Mesoporous Mater. 211 (2015) 64–72.
[25] J. Verduijn, A. Bons, M. Anthonis, L. Czarnetzki, Int. Pat. Appl., PCT WO 96/01683.
[26] G. Sotelo, Hidráulica De Canales, 1st ed., UNAM, México, 2002.
[27] J. Cravillon, R. Nayuk, S. Springer, A. Feldhoff, K. Huber, M. Wiebcke, Chem. Mater. 23 (2011) 2130–2141.
[28] S. Venna, J. Jasinski, M. Carreon, J. Am. Chem. Soc. 132 (2010) 18030–18033.
[29] X. Zhang, Z. Qu, F. Yu, Y. Wang, Chin. J. Catal. 34 (2013) 1277–1290.
[30] R. Houk, B. Jacobs, F. El Gabaly, N. Chang, A. Talin, D. Graham, S. House, I. Robertson, M. Allendorf, Nano Lett. 9 (10) (2009) 3413–3418.
[31] S. Salomons, R. Hayes, M. Votsmeier, A. Drochner, H. Vogel, S. Malmberg, J. Gieshoff, Appl. Catal., B 70 (2007) 305–313.
[32] J. Zamaro, N. Pérez, E. Miró, C. Casado, B. Seoane, C. Téllez, J. Coronas, Chem. Eng. J. 195 (196) (2012) 180–187.
[33] Y. Sohn, J. Mol. Catal. A: Chem. 379 (2013) 59–67.
[34] J. Fernández-Bertrán, M. Hernández, E. Reguera, H. Madeira, J. Rodriguez, A. Paneque, J. Llopiz, J. Phys. Chem. Solids 67 (2006) 1612–1617.
[35] J. Yao, R. Chen, K. Wang, H. Wang, Microporous Mesoporous Mater. 165 (2013) 200–204.
[36] V. Kaushik, J. Electron. Spectrosc. Relat. Phenom. 56 (1991) 273–277.
[37] M. Biesinger, L. Lau, A. Gerson, Roger St.C. Smart, Appl. Surf. Sci. 257 (2010) 887–898.
[38] A. Dhakshinamoorthy, H. Garcia, Chem. Soc. Rev. 41 (2012) 5262–5284.